The Geographical Journal of Nepal
Vol. 17: 23-52, 2024
DOI: https://doi.org/10.3126/gjn.v17i01.63934
Central Department of Geography,
Tribhuvan University, Kathmandu, Nepal

Landslide susceptibility mapping of the main boundary thrust region in Thungsingdanda-Bandipur section of Nawalparasi and Palpa Districts, Gandaki and Lumbini Provinces, Nepal

Kabi Raj Paudyal*, Rupendra Maharjan, Birat Shrestha
Central Department of Geology, Tribhuvan University, Kathmandu, Nepal.
*Corresponding email: kabiraj.paudyal@cdgl.tu.edu.np

Received: 18 December, 2023; Accepted: 08 January, 2024; Published: March,2024

Abstract
This research assesses the results of a landslide susceptibility analysis employing frequency ratios (FR). It was conducted in collaboration between CNES/Airbus and Maxar Technologies using Google Earth. Landslides in the Thungsingdanda-Bandipur area were identified through imagery with a 50 cm spatial resolution. A comprehensive dataset for training and testing was established based on the landslide inventory. Nine causative variables: slope, aspect, relief, distance from the stream, distance from the road, curvature, distance from the thrust, geology, and land use were used. FR ratings were assigned to these causative variables based on training events. The resultant landslide susceptibility map was generated by integrating causative variables with their respective FR ratings. The validation rate, determined using the ROC-AUC curve, was found to be 82.2 percent. Notably, distance from the thrust (MBT), land use, and distance from the road emerged as the more influential factors among the nine causative variables in landslide occurrences.

Keywords: landslide susceptibility, frequency ratio, geology, Nepal

INTRODUCTION
Nepal's hilly regions are characterized by rugged topography, frequent seismic activity, and seasonal monsoon rains, rendering them susceptible to various geohazards. Among these, landslides pose a significant and dynamic threat in steep terrains, with potentially far-reaching and lasting socioeconomic implications. The prevalence of deep and steep

river valleys in central Nepal can be attributed primarily to the geomorphic and tectonic history of the Nepal Himalayas (Hasegawa *et al.,* 2008). Numerous landslides, both large and small in scale, have taken place in these regions. The long-term stability of the slopes could be at risk, particularly in seismic-prone areas such as Nepal, due to earthquakes (Taylor & Burns, 2005).

Figure 1

Location map - Thungsingdanda-Bandipur section

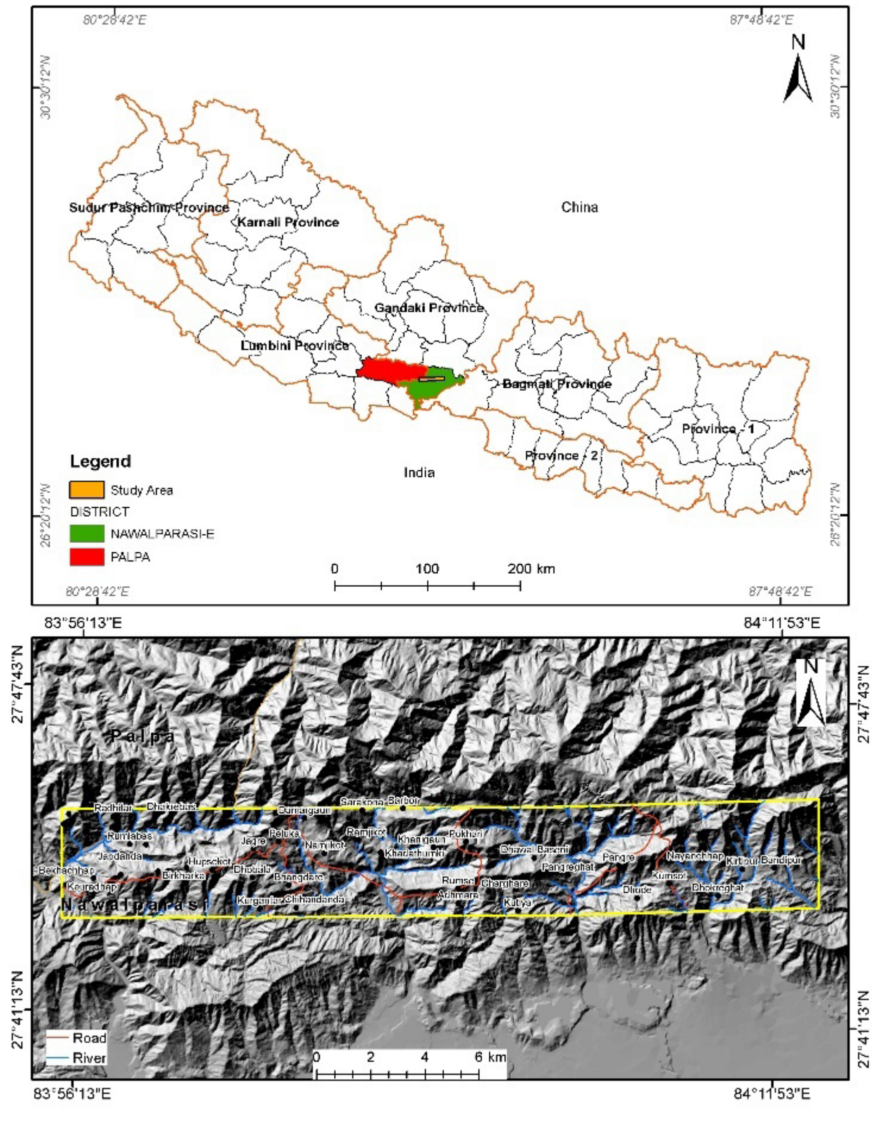

The main boundary thrust region in Nepal is the prime region of landslides and is highly susceptible to landslides. The selected research site, Thungsingdanda-Bandipur, is situated on the border of Nepal's Nawalparasi and Palpa districts (see Figure 1). This area is predisposed to landslides due to its rugged and dissected topography, coupled with the presence of a master thrust of the Himalaya, the Main Boundary Thrust (MBT). The elevation within the region varies from 336 m to a maximum of 1500 m, covering a total study area of 61.48 sq. km. The geographical boundaries of the study area extend from 493153.13m to 521097.54m East and 3071653.18m to 3066618.07m North. Local roads connected to Mahendra Rajmarg provide access to the study area. Owing to the presence of the MBT, steep slopes, rugged topography, and fragile rock conditions, the Thungsingdanda-Bandipur region is susceptible to various types of slope instability.

Methodology

In the process of mapping landslide susceptibility, it is crucial to recognize that factors contributing to landslides significantly impact the spatial occurrence of such events. Moreover, the inference is that future landslides are likely to occur under conditions like those that led to past landslides (Lee & Talib, 2005). In this study, Frequency Ratio (FR) method was employed to delineate the susceptibility of the area to landslides.

Over the past few decades, numerous scholars have developed effective techniques for producing precise landslide susceptibility maps. Examples of these approaches include frequency ratio (Goetz *et al.,* 2015; Budha *et al.,* 2016; Hong *et al.,* 2016; Lee *et al.,* 2016; Paudyal & Maharjan, 2022; (Neupane *et al.,* 2023), logistic regression (Chen *et al.,* 2017; Steger *et al.,* 2016); decision trees (Lee & Park, 2013; Pradhan, 2013; Tsangaratos & Ilia, 2016); fuzzy logic (Feizizadeh *et al.,* 2014; Park *et al.,* 2014; Pradhan, 2011), neurofuzzy systems (Pradhan, 2013; Aghdam *et al.,* 2016; Lee *et al.,* 2015); support vector machines (Pradhan, 2013; Peng *et al.,* 2014; Lee *et al.,* 2017; Tien Bui *et al.,* 2017); artificial neural networks (Conforti *et al.,* 2014; Pradhan & Lee, 2010; Tsangaratos & Benardos, 2014); and multimethod approaches (Althuwaynee *et al.,* 2016; Pham *et al.,* 2016; Pradhan, 2010; Yalcin *et al.,* 2011). In this study, the effectiveness of the landslide susceptibility assessment was evaluated using the frequency ratio (FR) method. The FR model offers the advantage of ranking causative variables based on their potential to trigger landslides. Additionally, it enables the assessment of whether a specific combination of causative factor values could pose a risk in the event of a landslide (Kannan *et al.,* 2013). The occurrence of landslides and debris flows is influenced by a multitude of variables. During intense rainfall, when soil moisture is high and soil strength is diminished, shallow landslides become more probable (Montgomery & Dietrich, 1994).

Figure 2

The approach employed in the analysis of landslide susceptibility mapping using FR method.

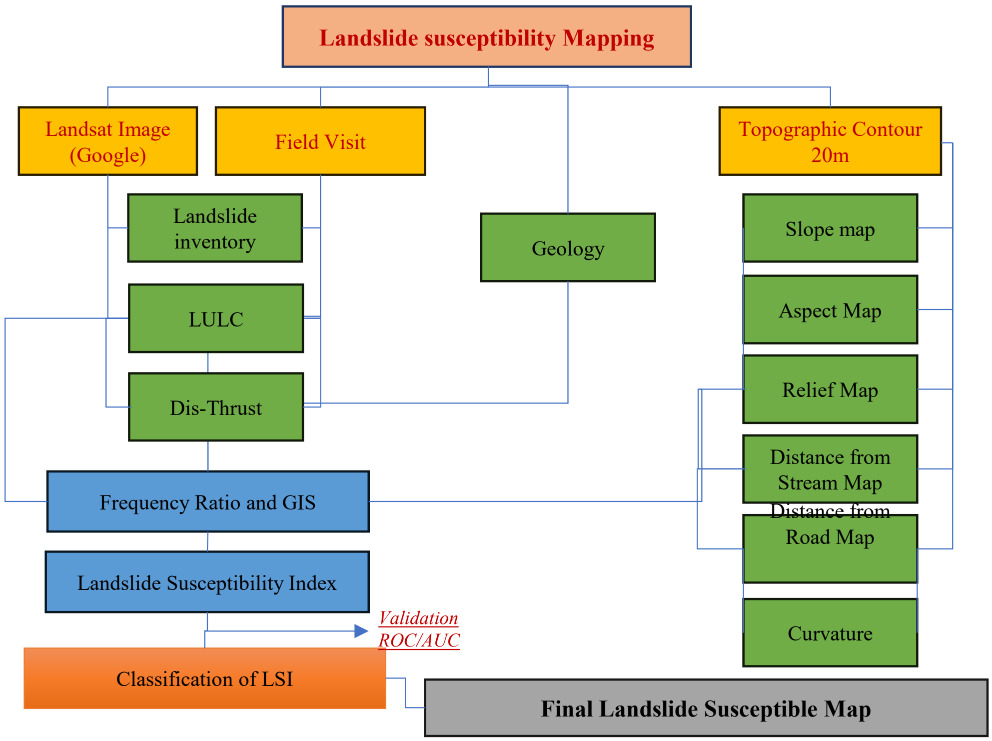

The process of creating a landslide inventory involved manually digitizing aerial photographs/satellite images having imagery resolution ranges from 15 meters of resolution to 15 centimeters (Landsat / Copernicus)from the Google Earth image dated March 2020, resulting in the identification of 104 landslides. This inventory was subsequently split into training (70% - 73%) and testing (30% - 31%) samples. The training sample was employed in developing the Landslide Susceptibility Index (LSI) model, while the testing sample was utilized to validate the model through the Receiver Operating Characteristic-Area Under the Curve (ROC-AUC) analysis in SPSS. The detailed methodology applied in the analysis is illustrated in Figure 2.

To conduct landslide susceptibility mapping, the creation of thematic data layers is essential (Camarinha *et al.,* 2014). Therefore, nine thematic layers, namely geology, slope, aspect, plan curvature, distance from the stream, distance from the thrust (MBT), distance from the road, relief, and land use and land cover, all with a resolution of 20m x

20m cells, were employed. A digital elevation model (DEM) derived from a triangulated irregular network (TIN) surface was utilized to generate topographic and hydrologic factors. The TIN was produced using ArcMap 10.4.1 and contour lines at 20m intervals from digital topographic maps. Various topographic and hydrologic factors, such as slope gradient, plan curvature, slope aspect, relief, and distance from the stream, were considered in the assessment of landslide susceptibility. The Land Use / Land Cover (LULC) map was crafted by digitizing the Google Earth imagery in ArcMap 10.4.1. Geological information and the location of the thrust (MBT) in the area were extracted from petroleum block data (Department of Mines &Geology, Government of Nepal). Additionally, a distance to MBT map was generated using the Euclidean distance algorithm.

Upon the completion of all nine-factor maps, the landslide inventory map was overlaid with each factor map, and tabulated data were generated. Subsequently, landslide susceptibility map was prepared through the application of the frequency ratio method (FR). The resultant Landslide Susceptibility Index (LSI) map was then classified into three zones: stable, quasi-stable, and unstable zones.

Frequency ratio method

To evaluate the potential for landslides, a comprehensive understanding of the distinct physical characteristics and mechanisms triggering landslides in each area is crucial. The frequency ratio serves as a quantitative approach for assessing landslide risk, employing GIS and geographical data (Lee & Talib, 2005; Chen *et al.,* 2016a, 2016b; Ding *et al.,* 2017). Widely utilized in landslide susceptibility mapping (Yilmaz, 2009; Reis *et al.,* 2012; Umar *et al.,* 2014; Chen *et al.,* 2016a; Wu *et al.,* 2016; Wang & Li, 2017), the frequency ratio (FR) technique establishes a quantified relationship between the landslide inventory and causative factors (Reis *et al.,* 2012). The derivation of the frequency ratio (FR) for each class of causative factors involves combining the landslide inventory map with the factor map using Eq. (1) (Mondal & Maiti, 2013; Fayez *et al.,* 2018).

$$FR = \frac{Npix(1) / Npix(2)}{\sum Npix(3) / \sum Npix(4)} \text{ ---Eq. (1)}$$

Where,

Npix(1) = The number of pixels containing landslide in a class

Npix(2) = Total number of pixels of each class in the whole area.

Npix(3) = Total number of pixels in a class of a parameter.

Npix(4) = Total number of pixels in the study area.

The accumulated frequency ratio is utilized to generate a Landslide Susceptibility Index (LSI) map, employing the formula presented in Eq. (2) (Lee & Talib, 2005).

$$LSI = FR_1 + FR_2 + FR_3 + FR_4 + \ldots\ldots\ldots + FR_n \text{-----------------------------------} \quad \text{Eq. (2)}$$

Results

Landslide inventory

Based on the Landsat images freely available on Google Earth and field visits, 104 landslides were mapped with a total area of 0.665 km^2 (Figure 3).During field visit, about 50 landslides were observed and verified the position, dimension, types, and causative factors.

Figure 3

Landslide inventory map showing both training & testing datasets

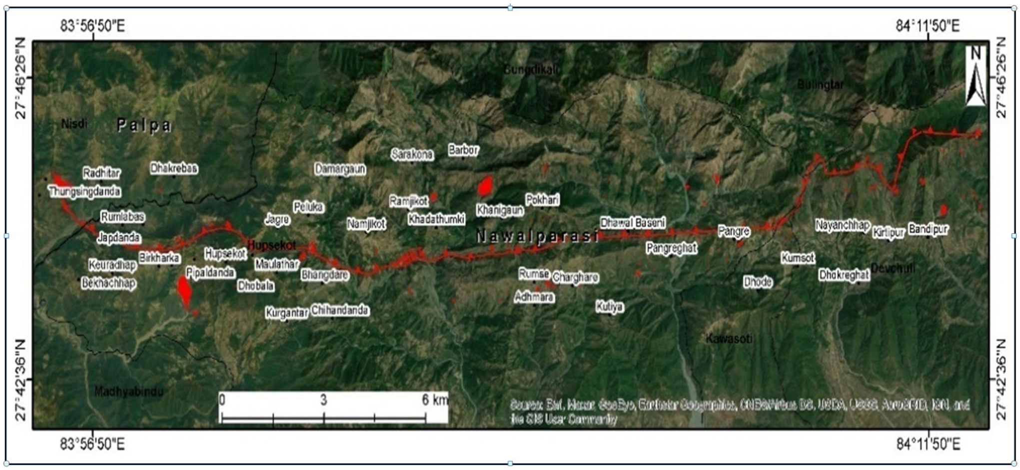

Landslide influencing factors

Land use land cover

The land cover map, depicted in Figure 4, was generated using an image classification tool. As illustrated in Table 1, the distribution of land cover in the Thungsingdanda-Bandipur region indicates that forests encompass 57.1% of the total area, agricultural land covers 14.06%, barren land occupies 0.4%, bushes account for 27.3%, rivers constitute 0.1%, and sand comprises 0.5% of the entire area. Analyzing the intersection of Land Use Land Cover (LULC) data with the current landslide occurrences reveals that 46.5% of the total landslides occur in forested areas, 33.4% in bush-covered regions, 11.1% in barren lands, 8.5% in agricultural areas, 0.5% in sandy areas, and none in river regions (Table 1).However, the density of landslide is high in the barren land of the study area.

In the land-use land cover category (refer to Table 2), the frequency ratio highlights that barren land exhibits a notably high susceptibility to landslides, with a substantial frequency ratio value of 30.38. In contrast, other classes such as forest (0.81), bushes (1.22), sand (1.07), agricultural land (0.58), and river (0) demonstrate comparatively lower frequency ratio values, with river having the least FR among them (Table 2).

Figure 4

Land-use map of the study area

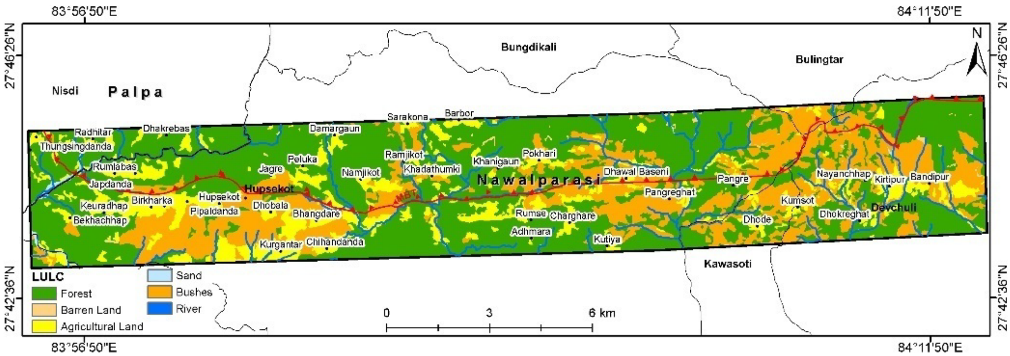

Geology

The geological map, sourced from the Department of Mines and Geology and illustrated in Figure 5, delineates the study area into eight major geological groups/units: Siwalik Group, Ramkot Formation/Surie Formation, Dhading Dolomite, Gawar Formation, and Amdanda Phyllite. According to Table 1, the Siwalik Group predominates in the study area, covering 58% of the total area, while exhibiting a landslide occurrence of 48.1%, with a corresponding frequency ratio (FR) of 0.83. The Ramkot Formation/Surie Formation, encompassing 37.6% of the area, displays a landslide occurrence of 51.2% and an FR value of 1.36. Dhading Dolomite, covering 1.1% of the total area, has an FR value of 0.55, constituting 0.6% of the total landslides. Amdanda Phyllite and Gawar Formation exhibit the lowest frequency ratios, with values of 0.07 and 0, respectively. These formations cover only 1.7% and 1.6% of the total study area and experience almost no landslides in the vicinity. This shows that there is strong lithological control on landslide initiation (Anup & Paudyal, 2020; Paudyal *et. al,* 2021).

Figure 5

Geological map of the Thungsingdanda-Bandipur

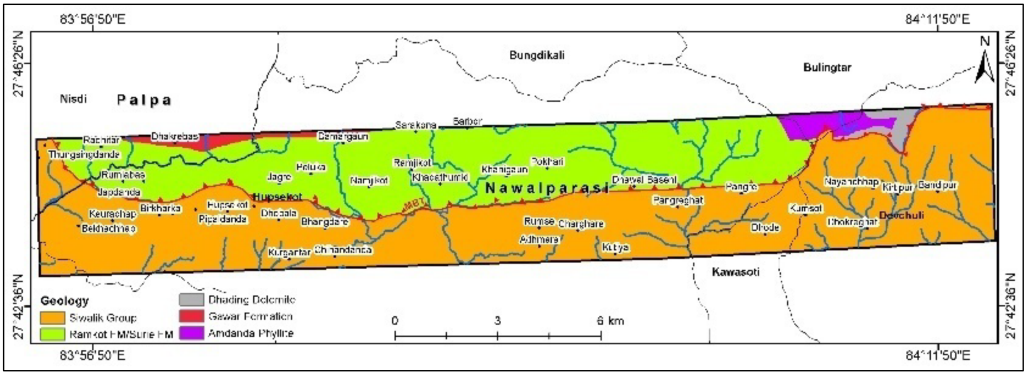

Distance to thrust (MBT)

This study incorporates the extrinsic parameter known as Distance to Thrust (MBT). The information on MBT from petroleum block no. 5 was acquired from the Department of Mines and Geology, Government of Nepal. Subsequently, the block underwent georeferencing, and the MBT location was delineated based on the map.

Utilizing the MBT and the Euclidean distance tool, the distance to thrust map (refer to Figure 6) was generated, illustrating the relationship of each cell to a source or set of sources based on straight-line distance. The map was then segmented into five distinct divisions.

Figure 6

Distance from thrust map of the study area

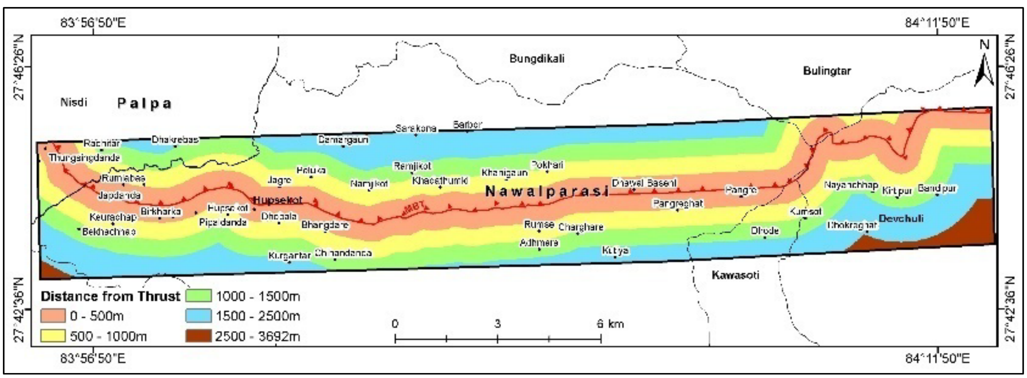

The investigation revealed that the most vulnerable zones to landslides were the nearest distances, i.e., 0 – 500m and 1000-1500m, as they accumulated the maximum percentage of all landslides (30.35% and 34.37%, respectively). This observation is substantiated by the Frequency Ratio table, indicating that these zones have the highest FR values of 1.12 and 1.52, respectively. Additionally, it was observed that there were no landslides at a distance of 2.5km from the thrust, with an associated FR value of 0.

Slope

The slope map (Figure 7) was created using a 20×20 Digital Elevation Model (DEM) through the Surface-Spatial Analyst Tool algorithm in ArcMap. The slope angles were categorized into eight classes using the equal interval classification method. As shown in Table 1, slope angles ranging from 00-100, 100–200, 200–300, 300–400, 400–500, 500–600, 600–700, and 700–820 constitute 4.94%, 14.64%, 31.39%, 35.32%, 12.81%, 0.94%, 0.08%, and 0.09% of the total study area, respectively. The corresponding landslide percentages in these slope categories are 1.9%, 10.1%, 28.3%, 41.8%, 16.3%, 1.6%, 0%, and 0%, respectively.

Terrain with a slope of 500–600 and 400–500 is identified as highly susceptible to landslides, with frequency ratios of 1.73 and 1.27, respectively. Conversely, terrain with a slope gradient of 00–100 is least prone to landslides, exhibiting a frequency ratio of 0.38 (Table 1). This is attributed to the lower incidence of landslides in that particular slope category.

Figure 7

Slope map of the Thungsingdanda-Bandipur

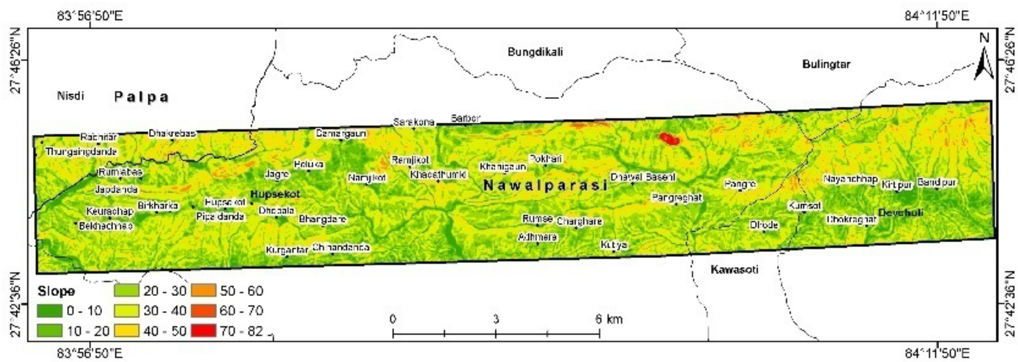

Aspect map

The aspect map (Figure 8) was generated using a 20×20 Digital Elevation Model (DEM) through the Surface-Spatial Analyst Tool algorithm in ArcMap. The aspect was categorized into eight classes, as illustrated in Table 1. The study area is characterized by a prevalence of south-facing slopes, covering 18.6% of the total study area. The second and third most dominant aspects are southwest and southeast facing, respectively. Notably, a significant proportion of landslides were observed in these aspects, with percentages of 16.14% for southeast, 21.66% for south, 29.15% for southwest, and 13.32% for west.

Figure 8

Aspect map of the Thungsingdanda-Bandipur region

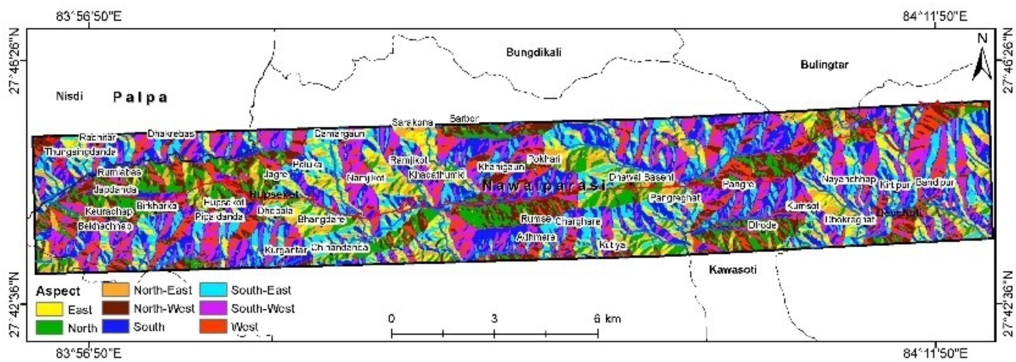

According to the frequency ratio indicated in Table 1, the southwest, west, south, and southeast aspects exhibit the highest frequency ratio values of 1.84, 1.20, 1.16, and 1.07, respectively. This implies that these aspects are comparatively more susceptible to landslides.

Figure 9

Relief map of the Thungsingdanda-Bandipur

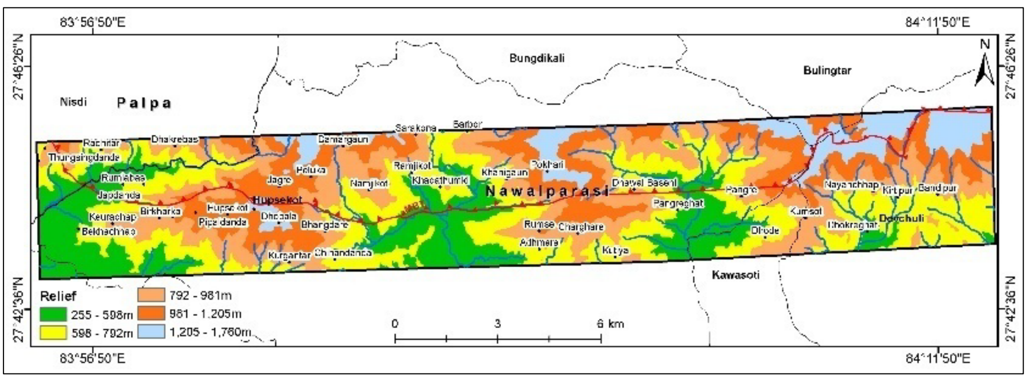

Relief map

The relief map, or elevation map, of the study area (Figure 9) was produced using a 20×20 m Digital Elevation Model (DEM). The lowest elevation recorded is 255m, while the highest elevation is 1760m. The relief map underwent classification into four classes via the natural break algorithm, as outlined in Table 1. Notably, the elevation range of 792 – 981m covers 25.7% of the total study area and is associated with 64.2% of total landslides, featuring the highest frequency ratio of 2.5.

Distance from stream

The proximity to streams is a significant factor in landslide susceptibility mapping, as areas near streams are more susceptible to landslides. Therefore, a distance to the stream map (illustrated in Figure 10) was generated using the Euclidean distance tool, which defines each cell's relationship to a source or set of sources based on straight-line distance. The map is classified into five interval classes. As indicated in Table 1, the area within the range of 0 to 50m constitutes 10.4% of the total study area and accounts for 6.3% of total landslides. Additionally, the region within a distance of 300–500m from the streams exhibits a high frequency ratio of 1.31, indicating a susceptibility to future landslides. This suggests that the "distance from stream" layer has a lesser impact on landslide occurrences around the streams.

Figure 10

Distance to stream map of the Thungsingdanda-Bandipur

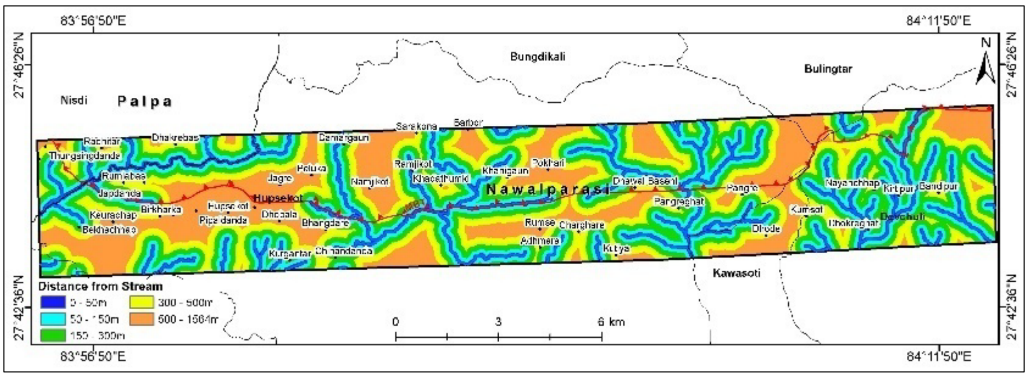

Curvature

Curvature, as depicted in Figure 11, represents the extent to which a curve deviates from being a straight line or a surface deviates from being a plane. The curvature map was created using a 20×20 m Digital Elevation Model (DEM) through the aspect algorithm of the Surface-Spatial Analyst Tool in ArcMap. Curvature is classified into concave, linear, and convex surfaces, as illustrated in Figure 10. According to Table 1, the study area exhibits a predominantly concave nature, covering 49.25% of the total area, while 50.09% of the area is characterized by convex topography, and the remaining 0.66% forms a linear or plane surface. Notably, the majority of landslides occurred in convex surfaces, with 50.1% of total landslides occurring in this zone. As the Frequency Ratio (FR) value for convex curvature (1.01) is higher than that of concave curvature (0.99), it is inferred that convex surfaces are more susceptible to landslides.

Figure 11

Curvature map of the Thungsingdanda-Bandipur

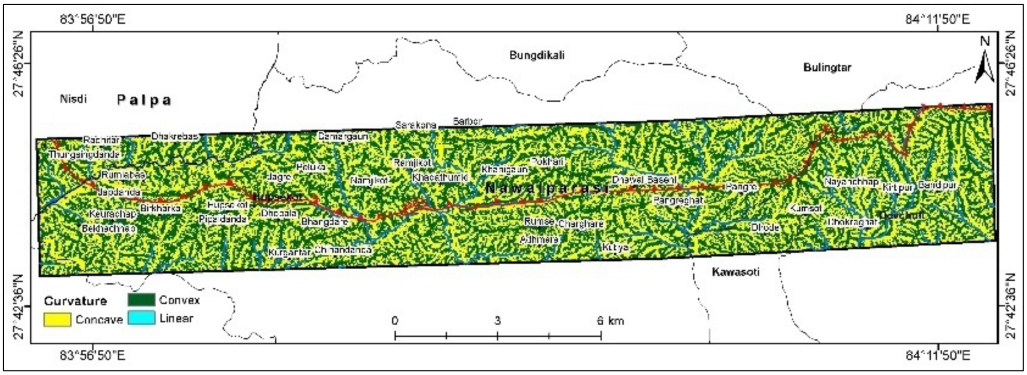

Distance from the road

The distance from the road map (depicted in Figure 12) was created using linear road data from the study area. The map illustrating the distance to the road (also Figure 12) was generated using the Euclidean distance tool, which outlines each cell's relationship to a source or set of sources based on straight-line distance. The distance from the road was classified into six groups: 0-50m, 50–150m, 150–300m, 300–500m, 500–1000m, and 1000–5663m. As indicated in Table 1, the area within the range of 0 to 50m constitutes 3.9% of the total study area and encompasses 1.3% of total landslides. Additionally, the region within distances of 150–300m and 300–500m from the road exhibits high frequency ratios of 1.40 and 1.30, respectively, indicating a susceptibility to future landslides. This suggests that the layer "distance from road" contributes less to landslides around constructed roads.

Figure 12

Distance from road map of the Thungsingdanda-Bandipur

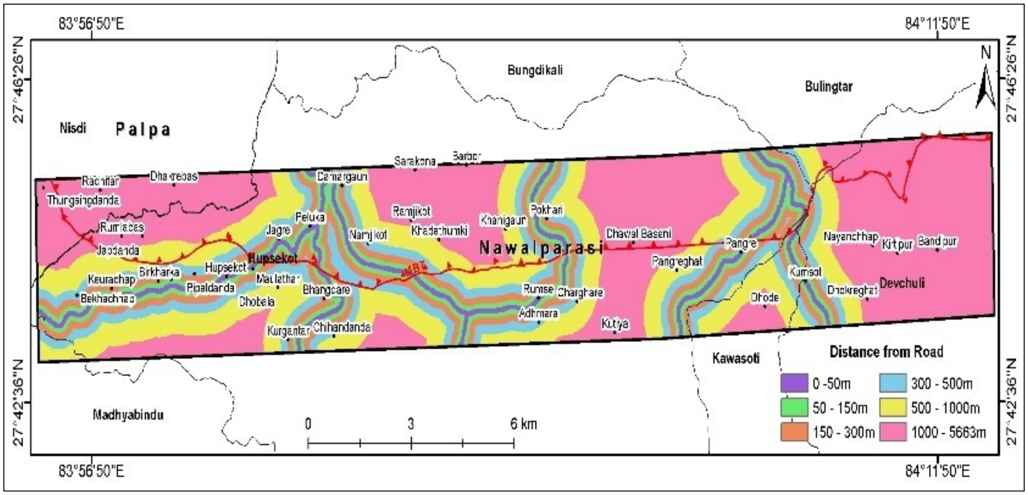

Lanslide susceptibility analysis

Landslide susceptibility Index map (LSI) was generated by combining all nine factor maps (Figure 13).

Final LSI = $PR_{d1}*FR_1 + PR_{d2}*FR_2 + PR_{d3}*FR_3 + PR_{d4}*FR_4 + \ldots\ldots + PR_{dn}*FR_n$----Eq.(3)

Were,

PR = Predictive ratio of each domain.

FR = Frequency ratio of each class of a domain (Influencing Factors).

Here the predictive ratio (PR) (Table 3) is the weight given to the domain or the influencing factor from table 1 which is calculated as in equation. 4 below:

PR = (Max RF – Min RF)/ (Min RF of Max RF – Min RF) - - - - - - - - - - - - - - Eq. (4)

Where RF stands for relative frequency. It is the ratio of FR of a class of a domain to total FR of the domain.

Table 1

Tabulation of domain with landslide inventory showing area coverage.

Domain	Class	Class Pixel	Area (sq. km)	% Class pixel	Landslide pixel	Area (sq. km)	% Landslide pixel
Slope	0 - 10	13708	5.48	4.92	31	0.012	1.86
	10 - 20	40293	16.12	14.46	169	0.068	10.14
	20 - 30	87463	34.99	31.39	471	0.188	28.25
	30 - 40	98440	39.38	35.32	697	0.279	41.81
	40 - 50	35693	14.28	12.81	272	0.109	16.32
	50 - 60	2611	1.04	0.94	27	0.011	1.62
	60 - 70	215	0.09	0.08	0	0.000	0.00
	70 - 82	251	0.10	0.09	0	0.000	0.00
Total		**278674**	**111.47**	**100.00**	**1667**	**0.667**	**100.00**
Distance to Thrust (MBT)	0 - 500m	75643	30.26	27.14	506	0.202	30.35
	500 - 1000m	67641	27.06	24.27	319	0.128	19.14
	1000 - 1500m	63038	25.22	22.62	573	0.229	34.37
	1500 - 2500m	65900	26.36	23.65	269	0.108	16.14
	2500 - 3692m	6454	2.58	2.32	0	0.000	0.00
Total		**278676**	**111.47**	**100.00**	**1667**	**0.667**	**100.00**
Land-use	Forest	159100	63.64	57.09	775	0.310	46.49
	Barren Land	1018	0.41	0.37	185	0.074	11.10
	Agricultural Land	40769	16.31	14.63	142	0.057	8.52
	Sand	1409	0.56	0.51	9	0.004	0.54
	Bushes	76185	30.47	27.34	556	0.222	33.35
	River	196	0.08	0.07	0	0.000	0.00
Total		**278677**	**111.47**	**100.00**	**1667**	**0.667**	**100.00**
Geology	Siwalik Group	161706	64.68	58.03	801	0.320	48.05
	Ramkot FM/Surie Formation	104894	41.96	37.64	854	0.342	51.23
	Dhading Dolomite	3027	1.21	1.09	10	0.004	0.60
	Gawar Formation	4374	1.75	1.57	0	0.000	0.00
	AmdandaPhyllite	4675	1.87	1.68	2	0.001	0.12
Total		**278676**	**111.47**	**100.00**	**1667**	**0.667**	**100.00**
Distance to Stream	0 - 50m	29120	11.65	10.45	105	0.042	6.30
	50 - 150m	49619	19.85	17.81	208	0.083	12.48
	150 - 300m	67476	26.99	24.21	419	0.168	25.13
	300 - 500m	64913	25.97	23.29	509	0.204	30.53
	500 - 1564m	67548	27.02	24.24	426	0.170	25.55
Total		**278676**	**111.47**	**100.00**	**1667**	**0.667**	**100.00**
Curvature	Concave	138857	55.54	49.83	821	0.328	49.25
	Linear	1790	0.72	0.64	11	0.004	0.66
	Convex	138026	55.21	49.53	835	0.334	50.09
Total		**278673**	**111.47**	**100.00**	**1667**	**0.667**	**100.00**
Aspect	North (0-22.5)	31816	12.73	11.42	27	0.011	1.62
	Northeast (22.5-67.5)	22341	8.94	8.02	96	0.038	5.76
	East (67.5-112.5)	29019	11.61	10.41	140	0.056	8.40
	Southeast (112.5-157.5)	42197	16.88	15.14	269	0.108	16.14
	South (157.5-202.5)	51910	20.76	18.63	361	0.144	21.66
	Southwest (202.5-247.5)	44095	17.64	15.82	486	0.194	29.15
	West (247.5-292.5)	30947	12.38	11.11	222	0.089	13.32
	Northwest (292.5-337.5)	26349	10.54	9.46	66	0.026	3.96
Total		**278674**	**111.47**	**100.00**	**1667**	**0.667**	**100.00**
Relief	255 - 598	50505	20.20	18.12	75	0.030	4.50
	598 - 792	83701	33.48	30.04	272	0.109	16.32
	792 - 981	71482	28.59	25.65	1070	0.428	64.19
	981 - 1,205	49329	19.73	17.70	195	0.078	11.70
	1,205 - 1,760	23657	9.46	8.49	55	0.022	3.30
Total		**278674**	**111.47**	**100.00**	**1667**	**0.667**	**100.00**
Distance from Road	0 -50m	10846	4.34	3.89	22	0.009	1.32
	50 - 150m	18789	7.52	6.74	76	0.030	4.56
	150 - 300m	26825	10.73	9.63	224	0.090	13.44
	300 - 500m	31715	12.69	11.38	246	0.098	14.76
	500 - 1000m	65247	26.10	23.41	331	0.132	19.86
	1000 - 5663m	125254	50.10	44.95	768	0.307	46.07
Total		**278676**	**111.47**	**100.00**	**1667**	**0.667**	**100.00**

Table 2

Frequency ratio of each class.

Domain	Class	Class Pixel	% Class pixel	Landslide pixel	% Landslide pixel	Frequency Ratio (FR)	Relative Frequency (RF)	RF (Non %)	Min RF	Max RF	Max-Min RF	(Max-Min) Min RF	PR
	0 - 10	13708	4.92	31	1.9	0.38	0.06	6.13					
	10 - 20	40293	14.46	169	10.1	0.70	0.11	11.37					
	20 - 30	87463	31.39	471	28.3	0.90	0.15	14.60					
	30 - 40	98440	35.32	697	41.8	1.18	0.19	19.20					
Slope	40 - 50	35693	12.81	272	16.3	1.27	0.21	20.66	0.06	0.21	0.15		11.31
	50 - 60	2611	0.94	27	1.6	1.73	0.28	28.04					
	60 - 70	215	0.08	0	0.0	0.00	0.00	0.00					
	70 - 82	251	0.09	0	0.0	0.00	0.00	0.00					
	Total	**278674**	**100.0**	**1667**	**100.0**	**6.17**	**1.00**	**100.00**					
	0 - 500m	75643	27.1	506	30.35	1.12	0.27	27.22					
	500 - 1000m	67641	24.3	319	19.14	0.79	0.19	19.19					
	1000 - 1500m	63038	22.6	573	34.37	1.52	0.37	36.98					
Distance to Thrust (MBT)	1500 - 2500m	65900	23.6	269	16.14	0.68	0.17	16.61	0.00	0.37	0.37		28.78
	2500 - 3692m	6454	2.3	0	0.00	0.00	0.00	0.00					
	Total	**278676**	**100.0**	**1667**	**100**	**4.11**	**1.00**	**100**					
	Forest	159100	57.1	775	46.5	0.81	0.02	2.39					
	Barren Land	1018	0.4	185	11.1	30.38	0.89	89.18					
	Agricultural Land	40769	14.6	142	8.5	0.58	0.02	1.71					
Land-use	Sand	1409	0.5	9	0.5	1.07	0.03	3.13	0.00	0.89	0.89		69.40
	Bushes	76185	27.3	556	33.4	1.22	0.04	3.58					
	River	196	0.1	0	0.0	0.00	0.00	0.00					
	Total	**278677**	**100.0**	**1667**	**100**	**34.06**	**1.00**	**100**					
	Siwalik Group	161706	58.0	801	48.1	0.83	0.29	29.44					
	Ramkot FM/Surie Formation	104894	37.6	854	51.2	1.36	0.48	48.39					
Geology	Dhading Dolomite	3027	1.1	10	0.6	0.55	0.20	19.63	0.00	0.48	0.48	0.01	37.65
	Gawar Formation	4374	1.6	0	0.0	0.00	0.00	0.00					
	AmdandaPhyllite	4675	1.7	2	0.1	0.07	0.03	2.54					
	Total	**278676**	**100.0**	**1667**	**100.0**	**2.81**	**1.00**	**100.00**					
	0 - 50m	29120	10.4	105	6.3	0.60	0.13	12.81					
	50 - 150m	49619	17.8	208	12.5	0.70	0.15	14.89					
	150 - 300m	67476	24.2	419	25.1	1.04	0.22	22.05					
Distance to Stream	300 - 500m	64913	23.3	509	30.5	1.31	0.28	27.85	0.13	0.28	0.15		11.71
	500 - 1564m	67548	24.2	426	25.6	1.05	0.22	22.40					
	Total	**278676**	**100.0**	**1667**	**100**	**4.71**	**1.00**	**100**					
	Concave	138857	49.8	821	49.3	0.99	0.327	32.65					
Curvature	Linear	1790	0.6	11	0.7	1.03	0.339	33.94	0.33	0.34	0.01		1.00
	Convex	138026	49.5	835	50.1	1.01	0.334	33.41					
	Total	**278673**	**100.0**	**1667**	**100.0**	**3.03**	**1.00**	**100.00**					
	North (0-22.5)	31816	11.4	27	1.62	0.1	0.02	1.93					
	Northeast (22.5-67.5)	22341	8.0	96	5.76	0.7	0.10	9.77					
	East (67.5-112.5)	29019	10.4	140	8.40	0.81	0.11	10.96					
	Southeast (112.5-157.5)	42197	15.1	269	16.14	1.07	0.14	14.49					
Aspect	South (157.5-202.5)	51910	18.6	361	21.66	1.16	0.16	15.81	0.02	0.25	0.23		17.99
	Southwest (202.5-247.5)	44095	15.8	486	29.15	1.84	0.25	25.05					
	West (247.5-292.5)	30947	11.1	222	13.32	1.20	0.16	16.30					
	Northwest (292.5-337.5)	26349	9.5	66	3.96	0.4	0.06	5.69					
	Total	**278674**	**100.0**	**1667**	**100.00**	**7**	**1.00**	**100.00**					
	255 - 598	50505	18.1	75	4.5	0.25	0.06	5.72					
Relief	598 - 792	83701	30.0	272	16.3	0.54	0.13	12.51	0.06	0.58	0.52		40.39
	792 - 981	71482	25.7	1070	64.2	2.50	0.58	57.61					
	981 - 1,205	49329	17.7	195	11.7	0.66	0.15	15.21					

Table 3

Weight of individual factor

Domain/Factor	PR	Weight
Curvature	1.00	100
Slope	11.31	1131
Distance to stream	11.71	1171
Distance to Road	14.74	1474
Aspect	17.99	1799
Distance to Thrust	28.78	2878
Geology	37.65	3765
Relief	40.39	4039
Landuse	69.40	6940

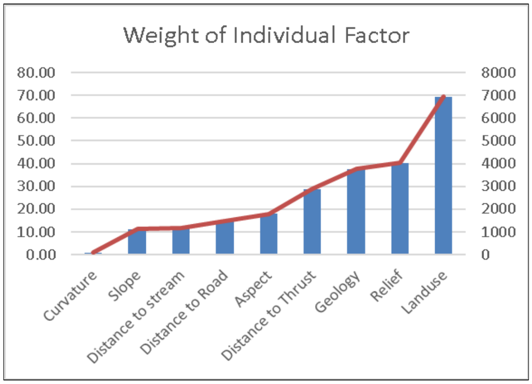

Figure 13

Landslide susceptibility Index map of the study area

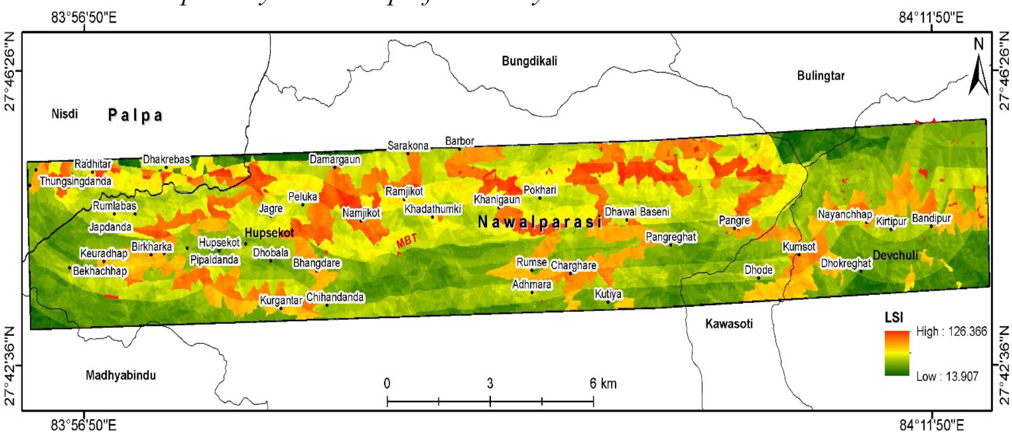

The Landslide Susceptibility Index (LSI) was developed employing Equation (2). For the classification of LSI data, the ROC/AUC curve was utilized. To assess the predictive capability of the proposed frequency method for identifying potential landslide zones, the LSI (landslide susceptibility index) underwent qualitative examination through success rate curves in IBM-SPSS Statistics 20. In the diagram above (refer to Figure 14), the area under the success rate curve (ROC/AUC) measures 0.796, signifying a prediction rate of 78.7% with an upper bound of 79.8%, validating the analysis. Regarding landslide potential, the success rate indicates that in 20% of the study area, there is a high rank, accounting for 65% of the total landslides in that area. Similarly, proposed GWP values of 40% and 50% can explain approximately 81% and 86% of all existing landslides, respectively. Consequently, three Groundwater Potential classes are established: stable zone (greater than 40%), quasi-stable zone (20-40%), and unstable zone (0-20%). Using these classes, the final landslide susceptibility map is generated, with LSI classified into three susceptibility zones—stable zone, quasi-stable zone, and unstable zone—with threshold values for the respective classes set at 41.09, 52.15, and 126.37, as indicated in Table 5, and the resulting final landslide susceptibility map depicted in Figure 15.

Figure 14

ROC/AUC curve of Thungsingdanda-Bandipur

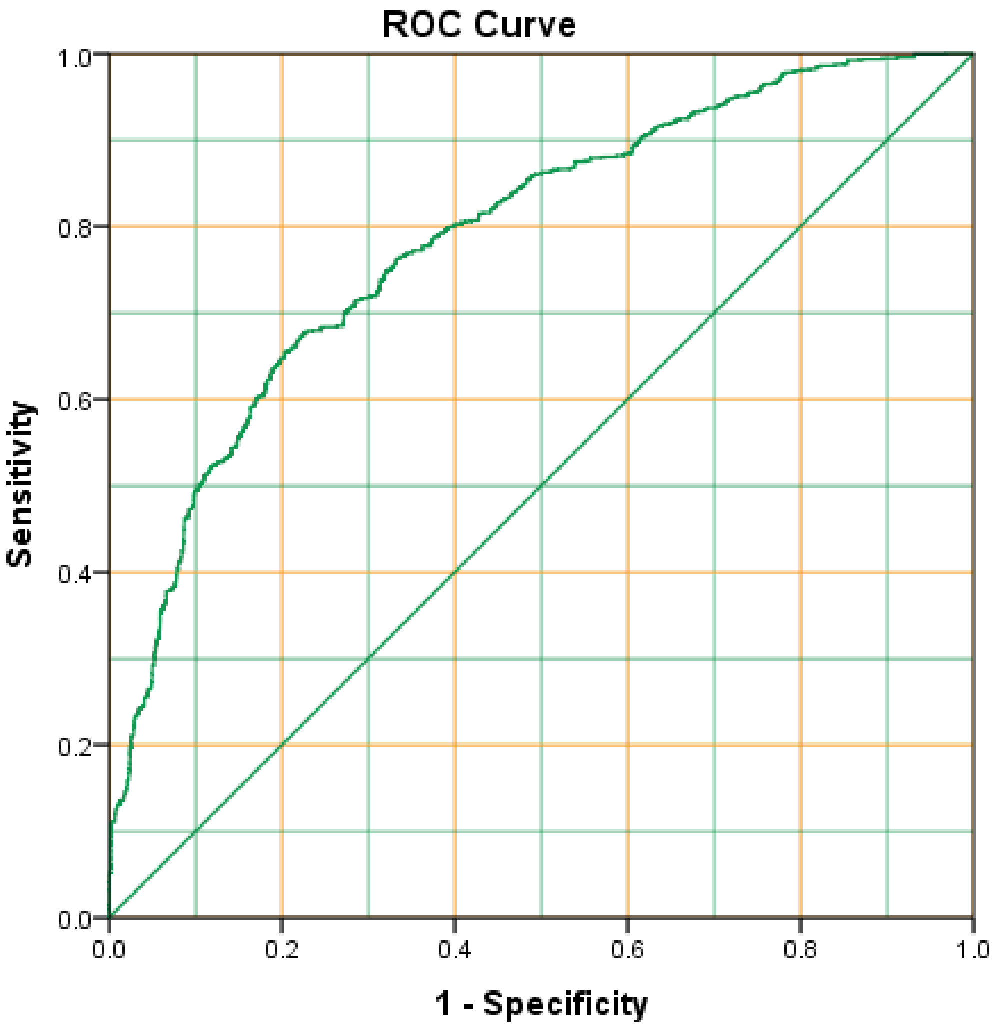

Table 4

Case processing summary

Slide	Valid N (listwise)
Positive[a]	1667
Negative	278023

Larger values of the test result variable(s) indicate stronger evidence for a positive actual state.

a. The positive actual state is 1.

Area Under the Curve

Test Result Variable(s): LSI

Area	Std. Error[a]	Asymptotic Sig.[b]	Asymptotic 95% Confidence Interval	
			Lower Bound	Upper Bound
.787	.006	.000	.776	.798

The test result variable(s): LSI has at least one tie between the positive actual state group and the negative actual state group. Statistics may be biased.

a. Under the nonparametric assumption

b. Null hypothesis: true area = 0.5

Table 5

Boundary value set for different susceptibility classes

Cumulative %	Class Name	LSI Upper Bound
60%	Stable Zone	**41.09**
80%	Quasi Stable Zone	**52.15**
100%	Unstable Zone	**126.37**

Table 6

Area coverage by different landslide susceptibility class.

Landslide Susceptibility				Classification Method
Class	Count	Area (sq. km)	Area %	
Stable	166792	66.72	59.99%	ROC/AUC Curve
Quasi Stable	55650	22.26	20.02%	
Unstable	55581	22.23	19.99%	
Total	**278023**	**111.21**	**100%**	

Figure 15

Landslide susceptibility map of the Thungsingdanda-Bandipur

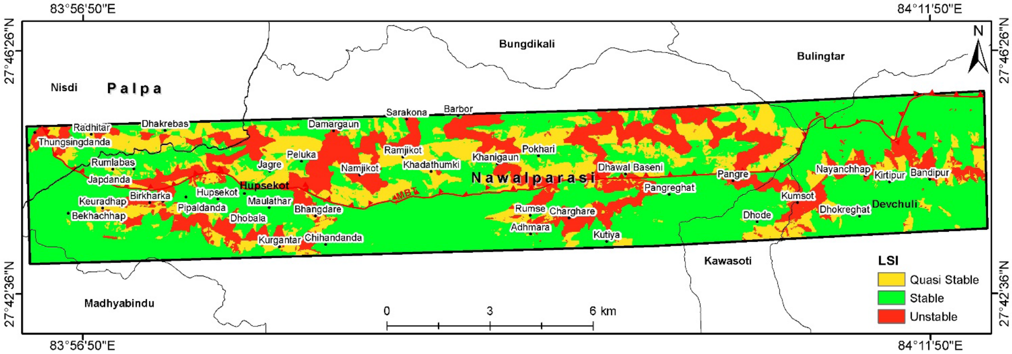

Figure 16

Bar-diagram showing the percentage of final susceptibility class in Thungsingdanda-Bandipur

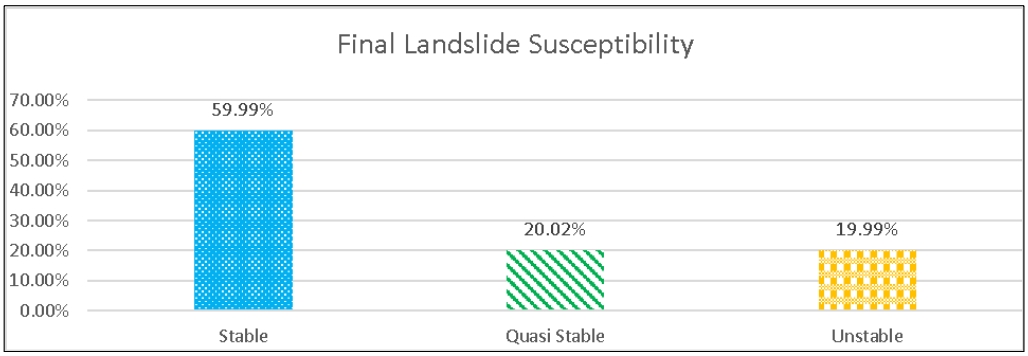

The outcome of the final susceptibility map (depicted in Figure 15), derived from the amalgamation of nine influencing factor maps, indicates that *Bandipur, Nayachhap, Kumsot, Pangre, Charghare, Namjikot, Damargaun, Birkharka, and Thungsingdanda* villages are situated in the unstable zone, rendering them prone to landslides. *Radhitar, Rumlabas, Japdanda, Keuradhap, Kurgantar, Ramjikot, Khadathumki, and Adhmara* fall within the quasi-stable zone. The remaining villages are classified as the stable zone. Among the total study area, 59.99% is designated as stable, encompassing villages such as *Kirtipur, Dhokreghat Dhode, Pangreghat, Dhawal Baseni, Kutiya, Rumse, Pokhari, Chihandanda, Maulathar, Hupsekot, Dhakrebas, and Bekhachhap*. Approximately 20.02% is identified as quasi-stable, while 19.99% of the study area is deemed unstable. Notably, one region is assessed as highly prone to landslides (refer to Table 6).

Discussion

Landslide causative factors

In this study, the selection of contributing factors was based on their presence or absence and their relative importance. The landslide conditioning factors encompassed geomorphological, anthropogenic, and extrinsic elements. Nine conditioning factors were considered to create the landslide susceptibility map: distance from thrust (MBT), aspect, slope, land use land cover, relief, distance from the stream, geology, distance from the road, and curvature. Table 1 provides the assigned weights for each class of causative factors. Geological structure and lithological factors have the most significant role to cause the landslide as in the other parts of the Nepal Himalaya (Acharya *et al,* 2023; K.C. *et al,* 2018).

The weights derived through the frequency ratio method highlight the significant impact of terrain slope on landslide distribution. Generally, landslide occurrences increase with an increase in terrain gradient (Paudyal & Maharjan, 2022). However, in our study area, many landslides are concentrated in the range of 50^{o} - $60^{o,}$ resulting in a high-frequency ratio of 1.73 and indicating heightened susceptibility to landslides (Table 1). Regions with slopes of 60^{o} - 70^{o} and 70^{o} - 82^{o} cover minimal areas and show no landslide presence, yielding respective FR values of 0.

According to (Chen *et al.,* 2017; Devkota *et al.,* 2013; Hong *et al.,* 2016) most of the landslides occurred on the slopes facing south and southeast. The frequency ratio for the aspect map indicates that southwest, south, west, and southeast-facing aspects have the highest frequency ratio values (Table 2) and are considered as prone to landslides in the study area. The southwest aspect boasts the maximum FR of 1.84, followed by the west with 1.20, and the west slope has an FR value of 1.16 (Table 1). Areas within the range of 0 – 50 m and 300 – 500 m from streams exhibit high frequency ratios of 0.6 and 1.31, respectively. This suggests that streams contribute less to landslide events in the study area. Among the land use land cover types, barren land has the highest FR of 30.38. Observing Table 1, it is evident that convex curvature surfaces in the study area are more susceptible to landslides, as they exhibit a high frequency of landslide occurrences with an FR value of 1.01. Furthermore, it was observed that most landslides occur in the Ramkot Formation, with an FR value of 1.36, followed by the Siwalik Group (Anup & Paudyal, 2020; Dahal & Paudyal, 2022) and Dhading Dolomite with FR values of 0.83 and 0.55, respectively. The distance from the road suggests that regions within 150–300 m are more susceptible to landslides, as the FR value is 1.40, compared to regions within the distance of 0–50 m (0.34). This contradicts with the previous study (Ayalew & Yamagishi, 2005) where they found that the effect of the road on landslides varies according to its role in the study area. while some researchers

(Seda, 2023) encountered landslides in areas up to 300 m, while other researchers found the most landslides occurred between 40 and 80 m .

Finally, the nearest distance from the thrust (MBT) has the second-highest percentage of landslides, with a frequency ratio value of 1.12 (ref to Paudyal & Maharjan, 2023). Consequently, the zone within the 0 – 500 m distance is the second most vulnerable to landslides, while the region within the distance of 1 km to 1.5 km is the most prone to landslides. This indicates that MBT has a moderate influence on triggering landslides in the study area.

Topographic parameters

The utilization of the Digital Elevation Model (DEM) is crucial in earthquake-induced landslide studies, as demonstrated by previous research (Kamp *et al.,* 2008; Wang *et al.,* 2015). While there is no direct correlation between elevation and landslide occurrence (Ercanoglu *et al.,* 2004), studies indicate an elevated probability of landslides at higher elevations. In this study, landslide concentration was most pronounced within the elevation range of 792m to 981m. Steepness of the slope stands as another significant topographic factor explored in landslide susceptibility studies (Wang *et al.,* 2015; Kamp *et al.,* 2008; Regmi *et al.,* 2016; Regmi *et al.,* 2010; Pradhan & Lee, 2010).The slope ranges from 0° to 82°.The highest landslide concentration was observed along the slope angle ranging 50° - 60° (Figure 7).

The aspect of the slope, influencing moisture retention and rock formation, is a critical factor in slope material properties and susceptibility to failure (Dai *et al.,* 2001). This association is often observed due to the prevalent river segment trends in the SW-SE direction, resulting in numerous landslides on slopes facing the river.

Surface undulation on the slope plays a pivotal role in triggering landslides, exerting a substantial influence on slope instability. In terms of curvatures, landslides are commonly distributed in both convex and concave slopes (Figure 11). Convex slopes, in particular, are prone to earthquake-induced landslides (Reneau & Dietrich, 1987). Moreover, the region within 150 – 300m from the road exhibits heightened susceptibility to landslides.

Anthropogenic factor

Land use is recognized as a significant factor in landslide conditioning, as changes in land-use patterns can impact vegetation cover, thereby influencing mechanical factors (such as soil strength and slope behavior) and hydrological factors (Greenway, 1987; van Westen *et al.,* 2003; Reichenbach *et al.,* 2014). Variations in land use distribution can stem from natural processes, human activities, or a combination of both. According to frequency ratio weight values, the association with barren land, which holds a weight of 30.38, is more pronounced compared to other land use classes. Our findings align with this correlation.

Conclusion

In this investigation, a Frequency Ratio model based on statistical methods was employed to assess the spatial likelihood of landslide occurrence, assigning weights to each factor layer based on their impact on landslides. The model efficiently predicted the probability of landslides, a conclusion substantiated by positive correlations between field conditions and model results. A total of 104 landslides were identified in the study.

The analysis revealed that land-use patterns, particularly the distance from these land use patterns, exert a significant influence on landslide occurrences. The geology factor map indicated a higher incidence of landslides in the Ramkot Formation and Siwalik Group. The Slope map highlighted a concentration of landslides in slope angles between 50^0 to 60^0, indicating a preference for higher slopes or increased relief. Slope angles less than 10^0 exhibited minimal contribution to landslide initiation. The results further indicated a prevalence of landslides on slopes facing south, southwest, and west, as suggested by the aspect map. This could be because these slope aspects face the sunlight directly which cause heating effect while at night same aspects has cooling effect making these slope weaker in long run resulting in landslide. The Curvature map emphasized the role of convex curvature in predicting landslides.

Examining the Relief map revealed an increase in landslide frequency up to an elevation of 981m, followed by a decline in the percentage of landslide-affected areas. Despite the dominance of agricultural and forested areas in the Thungsingdanda-Bandipur region, the susceptibility analysis pointed to barren land (land where plant growth may be sparse, stunted, or contains limited biodiversity)as more vulnerable to landslides.

The study also identified a direct correlation between distance from the thrust and landslide events. The area around the Main Boundary Thrust (MBT) zone within the 0 – 500m distance range accounted for 30.5% of total landslides. Statistical analysis of the susceptibility map, generated using the Frequency Ratio model, emphasized that the maximum landslide distribution occurred in the distance from the road range of 150 – 300m, suggesting a limited contribution of roads to landslide occurrence in the study area. Among the factors analyzed, land use, relief, and distance to the thrust were identified as major contributors to landslide initiation in the Thungsingdanda-Bandipur region.

The research study on landslide susceptibility mapping at Thungsingdanda-Bandipur region carries significant implications for risk management and sustainable development. The identification of high susceptibility areas provides a foundation for targeted mitigation strategies, guiding interventions such as slope stabilization and vegetation cover enhancement to minimize potential damage. The findings inform land use planning, influencing zoning regulations and development plans, while also contributing to the establishment of early warning systems for timely evacuation and risk reduction. Engineers and planners can utilize the susceptibility mapping to design resilient infrastructure, taking into account factors like slope stability. Moreover, the study emphasizes the importance of environmental conservation in mitigating landslide risks, promoting sustainable land management practices. Community awareness and education efforts can be tailored based on the research, empowering residents to take preventive measures. The findings are also valuable for insurance companies and risk assessors, aiding in the development of accurate risk models that influence premiums and coverage. The research informs government policies related to land use, construction standards, and disaster management, shaping regulations that enhance regional resilience. It highlights the need for continued research and monitoring, addressing knowledge gaps and guiding future initiatives. Additionally, the study's international relevance fosters collaboration, sharing knowledge and best practices with other regions facing similar challenges.

Acknowledgements

The authors express their gratitude to the Central Department of Geology, Tribhuvan University, for generously supplying the requisite field equipment and research facilities essential for the successful execution of this study. Appreciation is also extended to the residents and communities for their valuable cooperation in facilitating accommodations and providing guidance for the field routes.

References

Acharya, M., Dhakal, R. P., & Paudyal, K.R., (2023). Application of frequency ratio method for landslide susceptibility mapping at the Thulo Lumpek area, Gulmi, Nepal. *Journal of Development Innovations, 7*(2), 56-76. Karma Quest International, www.karmaquest.org/journal

Aghdam, I.N., Varzandeh, M. H. M., & Pradhan, B. (2016). Landslide susceptibility mapping using an ensemble statistical index (Wi) and adaptive neuro-fuzzy inference system (ANFIS) model at Alborz Mountains (Iran). *Environmental Earth Sciences*, *75*, 553. https://doi.org/10.1007/s12665-015-5233-6

Althuwaynee, O. F., Pradhan B., & Lee S. (2016). A novel integrated model for assessing landslide susceptibility mapping using CHAID and AHP pair-wise comparison. *International Journal of Remote Sensing*, *37*(5), 1190–1209. https://doi.org/10.1080/01431161.2016.1148282

Ayalew, L., & Yamagishi, H. (2005). The application of GIS-based logistic regression for landslide susceptibility mapping in the Kakuda-Yahiko Mountains, Central Japan. *Geomorphology*, *65*, 15–31.

Budha, P.B., Paudyal, K.R., & Ghimire, M. (2016). Landslide susceptibility mapping in eastern hills of Rara Lake, western Nepal. *Journal of Nepal Geological Society, 50*(1), 125-131.

Camarinha P.I.M., Canavesi V., & Alval´a R.C.S. (2014). Shallow landslide prediction and analysis with risk assessment using a spatial model in a coastal region in the state of Sao Paulo, Brazil. *Natural Hazards and Earth System Sciences*, *14*, 2449–2468, https://doi.org/10.5194/nhess-14-2449-2014

Chen, W., Chai, H., Sun, X., Wang, Q., Ding, X., & Hong, H. (2016a). A GIS-based comparative study of frequency ratio, statistical index and weights-of-evidence models in landslide susceptibility mapping. *Arabian Journal of Geosciences*. *9* (3), 204.

Chen, W., Pourghasemi, H. R., Kornejady, A., & Zhang, N. (2017). Landslide spatial modeling: Introducing new ensembles of ANN, MaxEnt, and SVM machine learning techniques. *Geoderma*, *305*, 314–327. https://doi.org/10.1016/j.geoderma.2017.06.020

Chen, W., Wang, J., Xie, X., Hong, H., Van Trung, N., Bui, D.T., Wang, G., Li, X. (2016b). Spatial prediction of landslide susceptibility using integrated frequency ratio with entropy and support vector machines by different kernel functions. *Environmental Earth Sciences, 75* (20), 1344.

Chen, W., Xie, X., & Wang, J. (2017). A comparative study of logistic model tree, random forest, and classification and regression tree models for spatial prediction of landslide susceptibility. *CATENA*, *151*, 147–160.

Conforti, M., Pascale, S., Robustelli, G., & Sdao, F. (2014). "Evaluation of prediction capability of the artificial neural networks for mapping landslide susceptibility in the Turbolo River catchment (northern Calabria, Italy). *CATENA*, *113*, 236–250.

Dai, F.C., Lee, C.F., Li.J., Xu, Z.W. (2001). Assessment of landslide susceptibility on the natural terrain of LantauIsland, Hongkong. *Environmental geology*, *40*(3), pp. 381–391. *https://doi.org/10.1007/s002540000163*

Dahal, A., and Paudyal, K.R. (2022). Mapping of Geological Sensitive Areas along the Budhi Khola Watershed, Sunsari/Morang Districts, Eastern Nepal Himalaya.© 2022. *Journal of Development Innovations, 6*(1), 44–68. www.karmaquest.org/.

Devkota, K., Regmi, A., Pourghase, H., Yoshida, K., Pradhan, B., & Ryu, I. (2013). Landslide susceptibility mapping using certainty factor, index of entropy and logistic regression models in GIS and their comparison at Mugling–Narayanghat road section in Nepal Himalaya. *Natural Hazards*, *65*(1), 135–165.

Ding, Q., Chen, W., Hong, H. (2017). Application of frequency ratio, weights of evidence and evidential belief function models in landslide susceptibility mapping. *Geocarto International, 32*(6), 619–639.

Ercanoglu, M., Gokceoglu, C., & Van Asch, T.W. (2004). Landslide susceptibility zoning north of Yenice (NW Turkey) by multivariate statistical techniques; *Natural Hazards*, *32*(1), 1–23.

Fayez L., Pham B.T., Solanki H.A., Pazhman D., Dholakia M.B., Khalid M., & Prakash I.(2018). Application of Frequency Ratio Model for the Development of Landslide Susceptibility Mapping at Part of Uttarakhand State, India. *International Journal of Applied Engineering Research, 13*(9), 6846-6854. *http://www.ripublication.com*

Feizizadeh B., Shadman M., Roodposhti, Jankowski P., & Blaschke T. (2014). A GIS-based extended fuzzy multi-criteria evaluation for landslide susceptibility mapping. *Computers and Geosciences*, *73*, 208–221.

Greenway, D.R. (1987). Vegetation and slope stability. ***In:*** Anderson M.G., Richards, K.S (eds.) *slope stability*, pp. 187–230.

Goetz J. N., Brenning A., Petschko H., & Leopold P. (2015). Evaluating machine learning and statistical prediction techniques for landslide susceptibility modeling. *Computers and Geosciences*, *81*, 1–11.

Hasegawa S, Nonomura A, Dahal R. K., Yuichi T, Haruki M, Yatabe R. (2008). Geomorphological approach for earthquake-induced landslides study. *International Conference on Disasters and Development 11*, 94–105.

Hong, H., Naghibi, S. A., Pourghasemi, H., & Pradhan, B. (2016). GIS-based landslide spatial modeling in Ganzhou city, China. *Arabian Journal of Geosciences*, *9*(2), 1–26.

Hong H., Pourghasemi H. R., & Pourtaghi Z. S. (2016). Landslide susceptibility assessment in Lianhua County (China): a comparison between a random forest data mining technique and bivariate and multivariate statistical models. *Geomorphology*, *259*, 105–118.

Kannan M., Saranathan E., & Anabalagan R. (2013). Landslide vulnerability mapping using frequency ratio model: a geospatial approach in Bodi-Bodimettu Ghat section, Theni district, Tamil Nadu, India, *Arabian Journal of Geosciences*, *6*(8), 2901–2913.

Kamp, U., Growley, B.J., Khattak, G.A., & Owen, L.A. (2008). GIS-based landslide susceptibility mapping for the 2005 Kashmir earthquake region. *Geomorphology*, *101*(4), 631–642.

K. C., J., Gautam, D., Neupane, P., & Paudyal, K.R. (2018). Landslide inventory mapping and assessment along the Ramche-Jharlang area in Dhading, Rasuwa, and Nuwakot districts, Lesser Himalaya, central Nepal. *Journal of Nepal Geological Society, 55*(Sp. Issue), 103-108. https://doi.org/10.3126/jngs.v55i1.22798

Lee, S., Hong, S., & Jung, H. (2017). A support vector machine for landslide susceptibility mapping in Gangwon province, Korea, *Sustainability*, *9*(1), 48.

Lee, S., & Park, I. (2013). Application of decision tree model for the ground subsidence hazard mapping near abandoned underground coal mines. *Journal of Environmental Management*, *127*, 166–176.

Lee, M.-J., Park, I., & Lee, S. (2015). Forecasting and validation of landslide susceptibility using an integration of frequency ratio and neuro-fuzzy models: a case study of Seorak mountain area in Korea, *Environmental Earth Sciences*, *74*(1), 413– 429.

Lee, M. J., Park, I., Won, J. S., & Lee, S. (2016). Landslide hazard mapping considering rainfall probability in Inje, Korea. *Geomatics, Natural Hazards and Risk*, *7*(1), 424–446.

Lee, S., & Talib, J.A. (2005). Probabilistic landslide susceptibility and factor effect analysis. *Environmental Geology*. *47* (7), 982–990.

Mondal, S., & Maiti, R., (2013). Integrating the analytical hierarchy process (AHP) and the frequency ratio (FR) model in landslide susceptibility mapping of Shiv-khola watershed. *International Journal of Disaster Risk Science*. *4*(4), 200–212.

Montgomery D.R. & Dietrich W.E.(1994). A physically based model for the topographic control on shallow land sliding. *Water Resources Research*, *30*(4), 1153–1171.

Neupane, A., Paudyal, K.R., Devkota, K.C., & Dhungana, P. (2023). Landslide susceptibility analysis using frequency ratio and weight of evidence approaches along the Lakhandehi Khola watershed in the Sarlahi District, southern Nepal. *Geographical Journal of Nepal*, *16*(01), 73–96. https://doi.org/10.3126/gjn.v16i01.53486 .

Neupane, A., & Paudyal, K.R. (2021). Lithological Control on Landslide in the Siwalik Section of the Lakhandehi Khola Watershed of Sarlahi District, South-Eastern Nepal. *Journal of Development Innovations, 5*(2), 44-65.

Park, I., Lee, J., & Saro, L. (2014). Ensemble of ground subsidence hazard maps using fuzzy logic Central. *European Journal of Geosciences*, *6*(2), 207–218.

Paudyal, K.R., & Maharjan, R. (2022). Landslide susceptibility mapping of the Main Boundary Thrust (MBT) region in Tinau-Mathagadhi Section of Palpa District, Lumbini Province. *Journal of Nepal Geological Society*. *63*, 99–108. *https://doi.org/10.3126/jngs.v63i01.50845.*

Paudyal, K.R., Devkota, K.C., Parajuli, B.P., Shakya, P., & Baskota, P. (2021). Landslide Susceptibility Assessment using open-source data in the far western Nepal Himalaya: A case study from selected local level units. *Journal of Institute of Science and Technology, 26*(2), 31-42 (2021) *ISSN: 2467-9062 (print), e-ISSN: 2467-9240* https://doi.org/10.3126/jist.v26i2.41327.

Peng, L., Niu, R.Q., Huang, B., Wu, X.L., Zhao, Y.N., & Ye, R.Q. (2014). Landslide susceptibility mapping based on rough set theory and support vector machines: a case of the Three Gorges area, China. *Geomorphology*, *204*, 287–301.

Pham, B.T., Tien Bui, D., Dholakia, M.B., Prakash, I., & Pham, H.V. (2016). A comparative study of least square support vector machines and multiclass alternating decision trees for spatial prediction of rainfall-induced landslides in a tropical cyclones area. *Geotechnical and Geological Engineering*, *34*(6), 1807–1824.

Pradhan, B.(2011). Manifestation of an advanced fuzzy logic model coupled with Geo-information techniques to landslide susceptibility mapping and their comparison with logistic regression modeling. *Environmental and Ecological Statistics*, *18*(3), 471–493.

Pradhan, B. (2013). A comparative study on the predictive ability of the decision tree, support vector machine, and neuro-fuzzy models in landslide susceptibility mapping using GIS. *Computers and Geosciences*, *51*, 350–365.

Pradhan, B., & Lee, S. (2010). Landslide susceptibility assessment and factor effect analysis: backpropagation artificial neural networks and their comparison with frequency ratio and bivariate logistic regression modelling. *Environmental Modelling and Software*, *25*(6), 747–759. https://doi.org/10.1016/j.envsoft.2009.10.016

Pradhan, B. (2010). Landslide susceptibility mapping of a catchment area using frequency ratio, fuzzy logic and multivariate logistic regression approaches. *Journal of the Indian Society of Remote Sensing, 38*(2), *301–320.*

Regmi, A.D., Dhital, M.R., Zhang, J.Q., Su, L.J., & Chen, X.Q. (2016), Landslide susceptibility assessment of the region affected by the 25 April 2015 Gorkha earthquake of Nepal. *Journal of Mountain Science*, *13*(11), 1941–1957. *https://doi.or g/10.1007/s1 1629-015-3688-2*

Regmi, N.R., Giardino, J.R., & Vitek, J.D. (2010). Modeling susceptibility to landslides using the weight of evidence approach: Western Colorado, USA. *Geomorphology*, *115*, 172–187. *https://doi.org/10.1016/j.geomorph.2009.10.002*

Reneau, S.L., & Dietrich, W.E. (1987). Size and location of colluvial landslides in a steep forested landscape; IAHSAISH publication, *165*, 39–48.

Reichenbach, P., Busca, C., Mondini, A.C., & Rossi, M. (2014). The influence of land use change on Landslide Susceptibility Zonation: The Briga catchment test site (Messina, Italy). *Environ Manage*, *54*(6), 1372-84. https://doi.org/10.1007/s00267-014-0357-0

Reis, S., Yalcin, A., Atasoy, M., Nisanci, R., Bayrak, T., Erduran, M., Sancar, C., & Ekercin, S. (2012). Remote sensing and GIS-based landslide susceptibility mapping using frequency ratio and analytical hierarchy methods in Rize province (NE Turkey). *Environmental Earth Sciences*. *66*(7), 2063–2073.

Seda, C. (2023). Linear parameters causing landslides: A case study of distance to the road, fault, drainage. *Kocaeli Journal of Science and Engineering*, *6*(2), 94–113. https://doi.org/https://doi.org/10.34088/kojose.1117817

Steger, S., Brenning, A., Bell, R., Petschko, H., & Glade, T. (2016). Exploring discrepancies between quantitative validation results and the geomorphic plausibility of statistical landslide susceptibility maps, *Geomorphology*, *262*, 8–23.

Taylor, M.J., & Burns, S.F. (2005). *Slope and seismic stability of Castel Lake Debris Dam. St. Helens, Washington.* (unpublished PhD dissertation), Norway, Edr. Senneset, Flaate and Larsen.

Tien Bui, D., Tuan, T.A., & Hoang, N.D. (2017). Spatial prediction of rainfall-induced landslides for the Lao Cai area (Vietnam) using a hybrid intelligent approach of least squares support vector machines inference model and artificial bee colony optimization, *Landslides*, *14*(2), 447–458.

Tsangaratos, P. & Benardos, A. (2014). Estimating landslide susceptibility through a artificial neural network classifier, *Natural Hazards*, *74*(3), 1489–1516.

Tsangaratos P., & Ilia, I. (2016). Landslide susceptibility mapping using a modified decision tree classifier in the Xanthi Perfection, Greece, *Landslides*, *13*(2), 305–320.

Umar, Z., Pradhan, B., Ahmad, A., Jebur, M.N., & Tehrany, M.S. (2014). Earthquake induced landslide susceptibility mapping using an integrated ensemble frequency ratio and logistic regression models in West Sumatera Province, Indonesia. *CATENA, 118*, 124–135.

Van Westen, C.J., Rengers, N., Soeters, R. (2003). Use of geomorphological information in indirect landslide susceptibility assessment. *Natural Hazards*, *30*, 399–411. https://doi.org/10.1023/B:NHAZ.0000007097.42735.9e

Wang, L.J., Guo, M., Sawada, K., Lin, J., & Zhang, J. (2015). Landslide susceptibility mapping in Mizunami City, Japan: A comparison between logistic regression, bivariate statistical analysis and multivariate adaptive regression spline models; *CATENA*, *135*, 271–282. https://doi.or g/10.1016/j.catena.2015.08.007

Wang, Q., & Li, W., 2017. A GIS-based comparative evaluation of analytical hierarchy process and frequency ratio models for landslide susceptibility mapping. *Physical geography*. *38*(4), 318–337.

Wu, Y., Li, W., Wang, Q., Liu, Q., Yang, D., Xing, M., Pei, Y., Yan, S. (2016). Landslide susceptibility assessment using frequency ratio, statistical index and certainty factor models for the Gangu County, China. *Arabian Journal of Geosciences*. *9*(2), 1–16.

Yalcin, A., Reis, S., Aydinoglu, A.C., & Yomralioglu, T. (2011). A GIS based comparative study of frequency ratio, analytical hierarchy process, bivariate statistics and logistics regression methods for landslide susceptibility mapping in Trabzon, NE Turkey. *CATENA*, *85*(3), 274–287.

Yilmaz, I. (2009). Landslide susceptibility mapping using frequency ratio, logistic regression, artificial neural networks and their comparison: A case study from Kat landslides (Tokat—Turkey). *Computers & Geosciences. 35*(6), 1125–1138.